Contents lists available at ScienceDirect

Medical Engineering and Physics

journal homepage: http://ees.elsevier.com

Simulation of lvot obstruction in transcatheter mitral valve-in-ring replacement

Salvatore Pasta [a,*], Stefano Cannata [b], Giovanni Gentile [c], Valentina Agnese [b], Michele Pilato [b], Caterina Gandolfo [b]

[a] Department of Engineering, University of Palermo, viale delle Scienze, Ed.8, 90128, Palermo, Italy
[b] Department for the Treatment and Study of Cardiothoracic Diseases and Cardiothoracic Transplantation, IRCCS-ISMETT, via Tricomi n.5, 90127, Palermo, Italy
[c] Department of Diagnostic and Therapeutic Services, Radiology Unit, IRCCS-ISMETT, via Tricomi n.5, 90127, Palermo, Italy

ARTICLE INFO

Article history:
Received 13 January 2020
Received in revised form 30 March 2020
Accepted 25 May 2020
Available online xxx

Keywords
Transcatheter mitral valve replacement
Finite-element analysis
Fluid-solid interaction

ABSTRACT

Left ventricular outflow tract (LVOT) obstruction is a feared complication of transcatheter mitral valve replacement (TMVR). This procedure leads to an elongation of LVOT in the left ventricle (namely, the neoLVOT), ultimately portending hemodynamic impairment and death. This study sought to understand the biomechanical implications of LVOT obstruction in two patients who underwent TMVR as an "off-label" application of the Edwards SAPIEN 3 (S3) Ultra transcatheter heart valve (THV). A computational framework of TMVR was developed to assess the neoLVOT area and quantify the sub-aortic flow structure. We observed that the annuloplasty ring serves as the key anchor zone of S3 Ultra THV. A good agreement was found between the numerically-predicted and CT-imaging measurements of neoLVOT area, with differences less than 10% in both patients. The pressure drop across the neoLVOT did not determine hemodynamic impairment in both patients. Quantification of structural and hemodynamic variables by computational modeling may facilitate more accurate predictions of the LVOT obstruction in TMVR, particularly for patients which are considered to have a borderline risk of obstruction

© 2020

1. Introduction

Transcatheter mitral valve replacement (TMVR) is an emerging treatment for patients with severe mitral valve disease at high risk for conventional mitral valve (MV) surgery. Clinical studies highlighted the efficacy and safety of TMVR in both purpose-built and off-label applications of transcathther heart valves (THV) for degenerated bioprosthesis, failed annuloplasty rings, mitral annular calcification [1-3]. TMVR can lead to an elongation of the outflow tract into the left ventricle whereas the pre-existing "native" left ventricular outflow tract (LVOT) confined by the most basal septum and the intervalvular fibrosa remains unchanged. The newly created elongation is the "neoLVOT" that is confined posteriorly by the deflected anterior mitral valve leaflet in failed annuloplasty rings, mitral annular calcification and functional severe mitral regurgitation or by the deflected bioprosthetic leaflets and the THV strut in degenerated bioprostheses [4].

The incidence of LVOT obstruction is a common post-procedural complication with a reported rate of 8.2% in valve-in-ring TMVR [5]. Although careful pre-procedural screening can reduce the risk of LVOT obstruction, a small outflow tract geometry can result in acute hemodynamic impairment and death. This is likely due to the fact that the current generation of THV are not specifically designed for MV implantation and have intrinsic design specifications that may make TMVR suboptimal. Predictors and procedural outcomes of LVOT obstruction demonstrated that a neoLVOT area of 180mm^2 is determinant of adverse events after TMVR for failed annuloplasty rings [6]. From a fluid-mechanics perspective, a narrow neoLVOT configuration is accompanied by an increase in the flow velocity and a pressure drop by the Bernoulli's principle. LVOT obstruction could be as either static or dynamic in nature; a) static LVOT obstruction determining sub-aortic stenosis; and b) dynamic LVOT obstruction resulting in systolic anterior MV motion.

This study aims to improve our understanding on the biomechanical implication of the neoLVOT in two patients who underwent TMVR in failed annuloplasty rings. A patient-specific computational framework was developed to first simulate the deployment of the Edwards SAPIEN 3 (S3) Ultra, and then assess hemodynamic alterations in correspondence of the neoLVOT. Post-TMVR computed tomography (CT) and transesophageal echocardiography (TEE) were adopted to compare predictions of neoLVOT area and evaluate left ventricular hemodynamic.

* Corresponding author: Salvatore Pasta, PhD, Professor of Industrial Bioengineering, Department of Engineering, University of Palermo,
E-mail address: salvatore.pasta@unipa.it (S. Pasta)

https://doi.org/10.1016/j.medengphy.2020.05.018
1350-4533/© 2020.

UNCORRECTED PROOF

2. Methods

2.1. TMVR procedure

Data were collected from two patients (A and B) underwent transapical transcatheter mitral valve-in-ring replacement in our hospital institution. TMVR was decided by the Heart Team on the basis of clinical considerations and because of the high surgical risk of patients. Patient A was a 70 years-old lady with multiple episodes of heart failure and history of surgical MV annuloplasty using the 28 mm 3D Sorin Memo 3D ring (Sorin Group Italia SrL, Saluggia, Italy). Patient B was a 71-years-old gentlemen with MV complications related to a previously treated minimally-invasive annuloplasty band ring (28 mm Sorin Memo 3D) in the context of moderate left ventricular dysfunction. Annulus dimensions used for sizing of the balloon-expandable S3 Ultra (Edwards Lifesciences, USA) were based on pre-operative CT measurements. TMVR was performed under general anesthesia with TEE echocardiography and fluoroscopy guidance where the S3 Ultra was advanced and deployed by slow inflation during rapid pacing (150–200 bpm). The device was positioned into the annuloplasty ring with 1/3 height into atrial portion while the remaining part was inside the ventricular portion as suggested by manufacturer guidelines.

Successful implantation of S3 Ultra was determined by post-TMVR CT imaging to evaluate the correct deployment and quantify the neoLVOT area whereas hemodynamic function was evaluated by TEE imaging. Patients were discharged as none of them reported any significant acute events and exhibited preserved neoLVOT area at CT imaging. The study was approved by our local ethics review committees, and patients gave informed consent to their inclusion in the study.

2.2. Computational analysis

The computational approach consisted of a finite-element analysis of S3 Ultra deployment in the left ventricle to assess MV displacement and quantify neoLVOT area. This was followed by a fluid-solid interaction (FSI) analysis to evaluate hemodynamic alterations in the LVOT obstruction induced by the protruded THV in the left ventricle. FSI was based on the smoothed-particle hydrodynamics technique in ABAQUS (v.2016, Dassault Systemes, FR) to simulate motion of both mitral and aortic valves.

2.3. Heart model

Pre-operative, electrocardiographically-gated CT images were processed by Mimics (v.21, materialise, BE) to reconstruct patient-specific heart anatomies as done previously by our group [7-11]. Spatial resolution of CT scans was 0.625 mm in the z-axis while spacing between slices was 1.25 mm. Specifically, the end-systolic cardiac phase was adopted to segment the heart at minimal chamber volume and thus smallest LVOT configuration. semiautomatic thresholding followed by manual mask editing was performed to reconstruct the left ventricle, left atrium and ascending aorta. Smoothing and refinement algorithms were used to improve mesh quality without altering the native heart geometry. Specifically, smoothing was performed with factor of Laplace filter of 0.12 and twelve iterations. Visual assessment done by comparing the original and smoothed meshes was adopted to avoid an extensive use of smoothing and refinement options. Annuloplasty ring geometries were based on simplified models due to the presence of CT-related artifacts. The centerline was automatically generated on the basis of the annuloplasty ring mask, and then the ring geometry was obtained by sweep protrusion of a cross-section circular curve along centerline. Native MV geometry was determined from parametric equations of valve leaflets in Rhino CAD software (v.5.5, McNeel & associates, SP), with length of anterior MV leaflet fixed by pre-TMVR CT measurements done at end-diastole [12]. Lengths of anterior MV leaflets were 22.8 mm and 15.6 mm for Patient A and B, respectively. A parametric modeling tool based on anatomic CT-derived measurements was used to design the aortic valve geometry according to a protocol developed by our group for the bicuspid aortopathy [13, 14].

Each geometry was meshed using ICEM software (ANSYS v.18, ANSYS, Inc., USA) and then the whole heart model was re-meshed at the interface to assure element continuity between the mitral annulus and valve leaflets and between the sinus and aortic valve leaflets. Specifically, left atrial and ventricular chambers and the ascending aorta were meshed with triangular shell elements (S3R). MV geometry was modeled with structured quadrilateral shell elements (S4), assuming thickness of 3.5 mm for MV leaflets. A combination of both tetrahedral and hexahedral solid elements were used to mesh ring models while structured solid elements were adopted to discretize aortic valve leaflets (thickness of 1 mm). Element size was derived after sensitivity analysis using three different levels of mesh refinement. To reduce computational cost due to various anatomical geometries, a mesh size between the medium and fine refinement levels was adopted. Table 1 summarizes element number for each anatomic component.

2.4. THV model

The S3 Ultra is manufactured by a cobalt-chromium alloy frame characterized by both inner and outer sealing skirts to minimize leakage at inflow portion of the device. After acquisition with high-resolution micro-CT scanner (Skyscan 1272, Bruker, USA), a reverse engineering approach was adopted to obtain the CAD model of 26 mm S3 Ultra. Nearly 60,000 structured-hexahedral solid elements with reduced integration and hourglass control (C3D8R) were used to discretize the metallic THV frame (Fig. 1A). Element number was derived from mesh sensitivity analysis reported previously by our group [15]. After crimping of the device, the sealing skirt was modeled closing cell geometries

Table 1
Material parameters adopted for each component of TMVR simulation; E = Young modulus; ν = Poisson coefficient; σ_y = yield stress; σ_{ult} = ultimate tensile stress; ε_p = plastic strain; μ = viscosity; D = density;.

	E (MPa)	ν	σ_y (MPa)	σ_{ult} (MPa)	ε_p	μ (Pa s)	D (kg/m^3)	Element Number (thousand)
Heart	4	0.49					1060	65.6–68.5
3D Memo Ring							8000	7.2–10.2
Aortic Valve	1	0.49					2000	5.4–5.5
Mitral Valve							1060	18.3–21.5
S3 Ultra	233×10^3	0.35	414	930	0.45		8000	59.2
Sealing Skirt	55	0.49	6.6	6.6	0.6		8000	3.5–3.7
S3 Leaflet	8	0.45					1060	10.5–12.5
Balloon	600	0.3					1060	62.8
SPH Fluid						3.7×10^{-3}	1060	301.2–320.1

UNCORRECTED PROOF

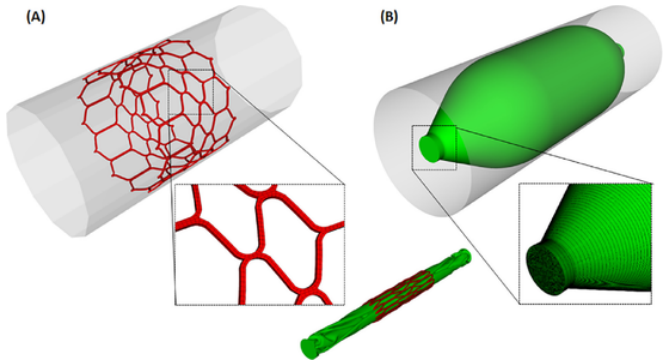

Fig. 1. (A) Initial S3 Ultra model showing the mesh and (B) initial balloon surface model prior to the deflation; inset shows the assembled balloon and crimped S3 Ultra.

with several surfaces build at mid-thickness of THV frame. These surfaces representing the sealing skirt at initial stress-free configuration were discretized with triangular shell elements and uniform thickness of 0.1 mm as measured on THV device. Bioprosthetic valve leaflets were modeled using a general 3D parametric geometry of the native aortic valve and meshed with structured solid elements to improve convergence of FSI solution during valve closing [16]. The balloon model developed here was based on the Edwards Novaflex delivery system, which was photographed at know scale. The balloon geometrical profile was realized in Rhino by revolution around the axis to create the balloon surface. The latter had thickness of 0.1 mm and was meshed with membrane elements (M3D4) to reduce computational cost (Fig. 1B).

2.5. Material models

For the sake of simplicity, the heart was modeled as a linear-elastic material with thickness of 4 mm and density of $D = 1060\ kg/m^3$. This could appear as a heavy assumption in our modeling approach but simulations shown that structural deformations were mainly governed by the quite stiff annuloplasty ring rather than the weak heart material model. The 3D Memo band ring is manufactured by Ni-Ti alloy so that material properties reported by Morganti et al. [17] (14 constants user material VUMAT available in ABAQUS) were adopted to model the ring. The anisotropic hyperelastic Holzapfel–Gasser–Ogden material model was adopted to characterize the mechanical behavior of human MV using the following descriptors: $C_1 = 0.12$ kPa, $C_2 = 13.6$, $k_1 = 11.0$ kPa, $k_2 = 84.8$ kPa, $k = 0.08$, $D = 1060\ kg/m^3$ [18]. Local coordinate systems were defined for each leaflet to include fiber orientation ($\theta = 13$ deg). For the S3 Ultra, Von Mises plasticity and isotropic hardening were adopted to model the cobalt-chromium alloy frame [19] while an elasto-plastic stress-strain model was used for the polyethylene terephthalate material of sealing skirt [20]. The aortic and bioprosthetic valve leaflets as well as the balloon were modeled with linear-elastic material properties ($D = 1060\ kg/m^3$). Table 1 summarizes material parameters of TMVR simulation.

2.6. Finite-element analysis of tmvr

Numerical analysis was performed in ABAQUS/Explicit solver to account for a non-linear problem including large deformation and complex contacts. Energy was monitored to ensure the ratio of kinetic energy to internal energy remained less than 10%, and a variable mass scaling technique was adopted to keep the time step less than 10^{-6}. Contacts among components were defined according to the general contact algorithm available in ABAQUS. A Rayleigh damping factor of 2000 was used for the heart, aortic and mitral valve leaflets to control the dynamic response of materials [16]. Simulations were performed on a 24 CPU workstation, and solutions were obtained after 3 days for the THV deployment and 6 days for the SPH analysis.

The S3 Ultra was crimped by a rigid dodecahedral surface gradually moved along the radial direction from the initial device diameter (ie, 23 and 26) to the final diameter of 4.5 mm (Fig. 1A). This surface was meshed using 1500 structured-quadrilateral surface elements with reduced integration and material density of $D = 7000\ kg/m^3$. A frictionless contact was defined between the crimping surface and the S3 Ultra while tie contact conditions were used to fix the skirt surfaces to the THV frame. Balloon deflation was simulated through radial displacement of a cylindrical crimper and by constraining distal ends in all directions (Fig. 1B). The deformed configuration of S3 Ultra THV was placed on the deflated balloon, and the assembly was then imported in the heart model (see inset of Fig. 1). Both frictionless and "hard" normal behavior contact conditions were adopted for the interaction between S3 Ultra and balloon.

For the expansion, the fluid-cavity-based model was employed to warrant a more realistic volume-controlled inflation and account for the over-expansion done during clinical procedure. Fluid-cavity material properties were manually calibrated by several simulations to ensure that the fluid filling volume leads to the nominal diameter expansion of S3 Ultra. As boundary conditions, distal ends of left atrium and ascending aorta were fixed in all directions while the expandable balloon was allowed to rotate during inflation.

After expansion, an elastic recoil was allowed by the contact release between the S3 Ultra THV and the expandable balloon. Before elastic recoil, prosthetic valve leaflets were mapped onto the implanted S3 Ultra device at initial stress-free closed configuration as described by others [21].

2.7. SPH modeling

The SPH numerical technique permits the modeling of extreme deformation and is ideal for simulating the fluid behavior during valve closure/opening. A reference density of $1060\ kg/m^3$ and viscosity of 0.0031Pa•s were adopted for blood properties using the pressure-density relation governed by the linear Hugoniot equation of state. For blood flow, the speed of sound is high compared to the bulk velocity of the blood so that an artificial sound speed of $c_0 = 145$ m/s was employed to avoid very small computational time steps while keeping density fluctuations within a small range and thus maintaining the incompressible flow behavior. Particles were uniformly distributed in the fluid domain with a spatial resolution of 0.5 mm in agreement with mesh sensitivity analysis carried out by Mao et al. [22]. Distal ends of both left atrium and ascending aorta were protruded 6-folds, and two rigid plates were then placed to apply pressure boundary conditions on the blood volume. Specifically, physiological pressure waveforms were generated to move blood particles in heart models (Fig. 2). Two cardiac cycles each of 0.8 s were simulated for each simulation, and the particle velocity field from the second cycle was analyzed. Contacts were enabled between particles and other components to allow FSI simulation. The interaction between SPH particles and deformable parts was based on the node-to-surface contact algorithm of ABAQUS/Explicit solver. The contact interaction in SPH is directly related to the no penetration boundary condition so that the combined effect of the smoothing kernel interpolation function near the wall and the node-to-surface contact interaction partially enforces the no-slip boundary condition.

3. Results

For Patient B with the 26 mm S3 Ultra, Fig. 3 shows different stages of S3 Ultra deployment where the balloon is inflated by the fluid-filling volume and thus drives THV expansion. The S3 Ultra is in contact at the beginning with the MV (images iii to iv) and later on

UNCORRECTED PROOF

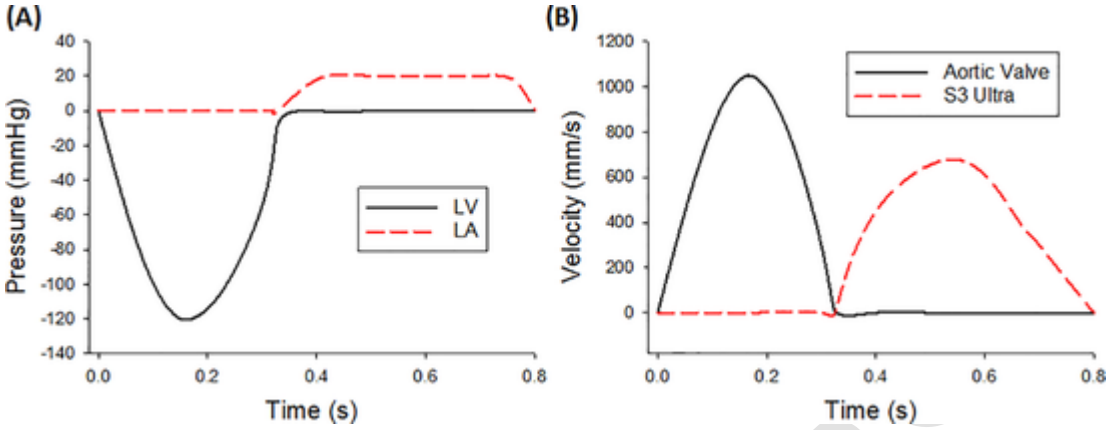

Fig. 2. (A) pressure and (B) corresponding velocity boundary conditions.

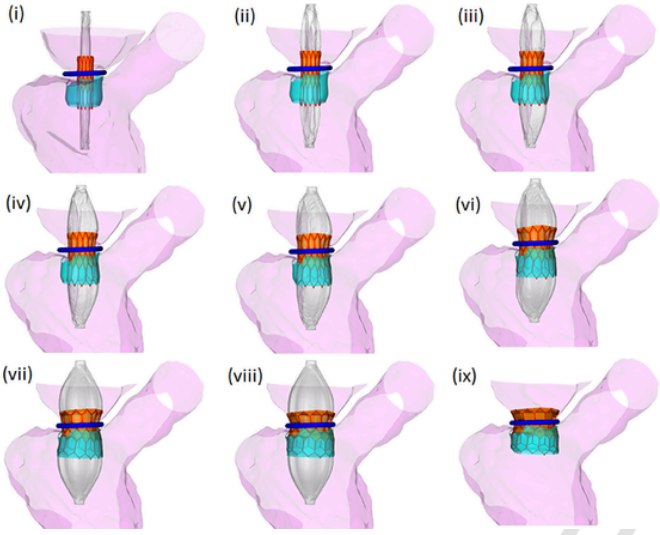

Fig. 3. Various stages of full THV deployment in the band ring; phase ix shows elastic recoil.

with the annuloplasty ring (images v). After THV deployment (images viii), the relaxing phase shows elastic recoil of all simulation components (image ix).

Qualitative comparison between angiography and simulation shows that the presence of the annuloplasty ring serve as the key anchor zone of 26 mm S3 Ultra, with attachment occurring between the first and second cell rows of THV frame (see Fig. 4). A good agreement between numerically-predicted and angiographic THV shapes can be observed in Fig. 4A and B. Fig. 4C shows local maxima of Von Mises stress in regions of stress concentration. Fig. 4D and E highlight maps of MV displacement induced by TMVR in Patient A and B, respectively. It can be observed that the anterior MV leaflet is displaced towards the inter-ventricular septum and, above all, the S3 Ultra frame is fully covered by the permanently-displaced MV leaflets. Patient A with the 23 mm S3 Ultra had a MV longer than the S3 Ultra (length of 1.9 mm, approximately).

For Patient B, Fig. 5 displays the neoLVOT and its area evaluation calculated according to the workflow suggested by Blanke and collaborators [4]. Specifically, a geometric centerline was created along the curvilinear axis of the neoLVOT and the aortic root (Fig. 5A). Then, the cross-sectional plane perpendicular to the centerline was developed in correspondence of the smallest neoLVOT region that was formed by the THV and the septum (Fig. 5B). For Patient B, TMVR simulation resulted in a neoLVOT area of 367.2mm^2 while the post-implantation CT imaging shown an area of 348.4mm^2 (ie, percentage error of 5.1%). For a Patient A, Fig. 6 illustrates the neoLVOT from a 3D view taken in the ascending aorta as compared to the cross sectional analysis of CT-derived neoLVOT area. A difference of 6.6% occurred between numerically-predicted (488.1mm^2) and clinically-derived (455.8mm^2) measurements of neoLVOT area.

Fig. 7 shows particle flow velocity of Patient A as assessed in a cross-sectional plane of 23 mm S3 Ultra at early systolic phase. Particle flow in the neoLVOT was characterized by a sub-aortic increased velocity, although not leading to a clinically-relevant hemodynamic impairment. Indeed, TEE echocardiography confirmed a preserved hemodynamic environment with a well-functioning THV and the absence of LVOT obstruction (see inset in Fig. 7). For Patient B, particle flow velocity is shown at different cardiac phases together with opening configurations of both mitral and aortic valves (Fig. 8). Simulations revealed an overall good opening of both THV and aortic valve leaflets, confirming no evidence of fluid-induced LVOT obstruction.

Fig. 9 illustrates the profile of the transmural pressure exerted on the anterior MV leaflet by the circulating flow particles. In diastole, the blood flowing from the left atrium to the left ventricle opens the prosthetic valve leaflets and determines a positive transmural pressure expanding the MV. During systolic acceleration, the transmural pressure becomes negative leading to a load force pushing the anterior MV leaflet to the S3 Ultra frame.

4. Discussion

Computational simulations as here proposed can offer predictive insights in the assessment of anatomical suitability and the risk of procedure-related complications of TMVR such as the LVOT obstruction. In this study, we described the structural mechanics and hemodynamic of the neoLVOT resulting from the S3 Ultra deployment in two patients at high surgical risk. We observed that the annuloplasty ring serves as the key anchor zone of S3 Ultra as confirmed by angiography. Post-TMVR CT assessment of neoLVOT area was found in agreement with that estimated by numerical simulations for both patients, with differences less than 10% between predictions and measurements. It should be noticed that the neoLVOT area of both patients was quite above the clinical cut-off value of 180mm^2, which is a prognostic value of adverse events [6]. This is likely a consequence of the screening on the anatomic suitability of native LVOT undertaken by our interventional cardiologists to pre-operatively minimize the risk of post-TMVR complications. During early systole, flow analysis revealed an increased sub-aortic blood flow and a drop in the pressure at the neoLVOT. However, the pressure drop along the neoLVOT may not fully account for the hemodynamic stress exerted on the THV device, and there is potential for the systolic flow to exert a transmural pressure on the anterior MV leaflet surface through the stent frame. We speculate that, especially in borderline pa-

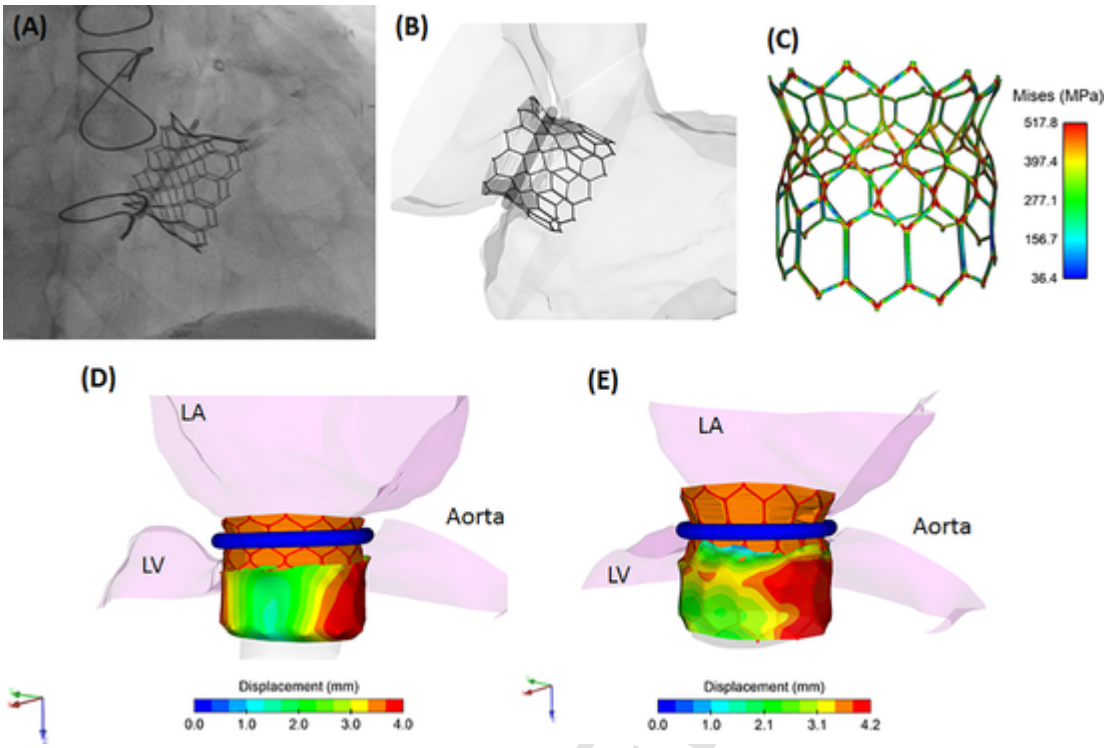

Fig. 4. (A) angiography and (B) simulation of 26 mm S3 Ultra deployed in Patient B; (C) Von Mises stress distribution of S3 Ultra; map of displacement of MV for (D) Patient A and (E) Patient B.

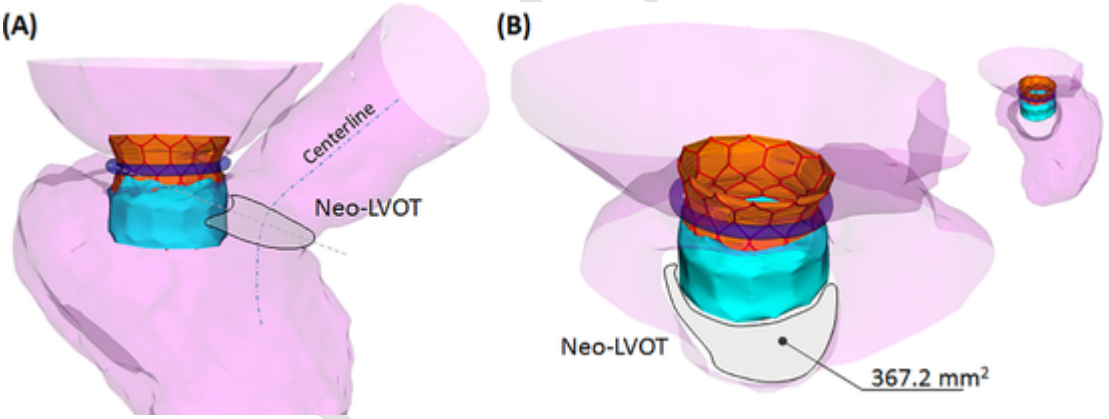

Fig. 5. (A) overview of calculation of neoLVOT area (B) 3D view of LVOT obstruction from the ascending aorta and corresponding neoLVOT area of Patient B.

tient cases, the transmural pressure could act by cantilevering the S3 Ultra in the context of a poor anchor zone and device specifications not based to engage the complex MV anatomy. Thus, quantification of the maximum velocity, pressure drop across the neoLVOT and transmural pressure may enable more accurate predictions of the LVOT obstruction in TMVR, particularly for patient anatomies which are considered to have a borderline risk of obstruction.

Several clinical studies have reported the anatomical conformation of neoLVOT after the implantation of THVs forcing the MV in an "open position" when adopted to repair degenerated bioprosthetic mitral valves, failed mitral annuloplasty rings, or patients with calcific MV disease [1-3]. The risk of life-threatening neoLVOT obstruction is increased when the aortic and mitral annular planes are acutely angulated rather than parallel, when the interventricular septum bulges toward the LVOT, when the anterior MV leaflet is elongated, and when the implant extends or flares into the left ventricle. Anterior MV leaflets longer than the implanted THV can also lead to MV prolapse into the neoLVOT or infolding into the THV by interfering with bioprosthetic heart valve opening or closing. In spite of such clinical studies, there is a very limited literature on the biomechanical implications of LVOT obstruction after TMVR. Most of computational studies on THV are related to transcatheter aortic valve implantation to determine the biomechanical interaction of the device with stenotic valve leaflets [23, 24] as well as the assessment of the risk of paravalvular leakage [25, 26]. In TMVR, Kohli and collaborators [27] performed a fluid-dynamic analysis where the prolonged THV was simulated by a rigid wall protrusion in the left ventricle and observed an increase in the flow velocity and pressure drop across the neoLVOT as here observed. Similarly, De Vecchi et al. [28] developed a parametric model of the protruded THV wall in the left ventricle and carried out several computational fluid-dynamic analyses for different degrees of LVOT obstruction. They found a significant increase in the left ventricular afterload for maintaining the cardiac output and suggested a deterioration of systolic flow efficiency proportional to the degree of LVOT obstruction. However,

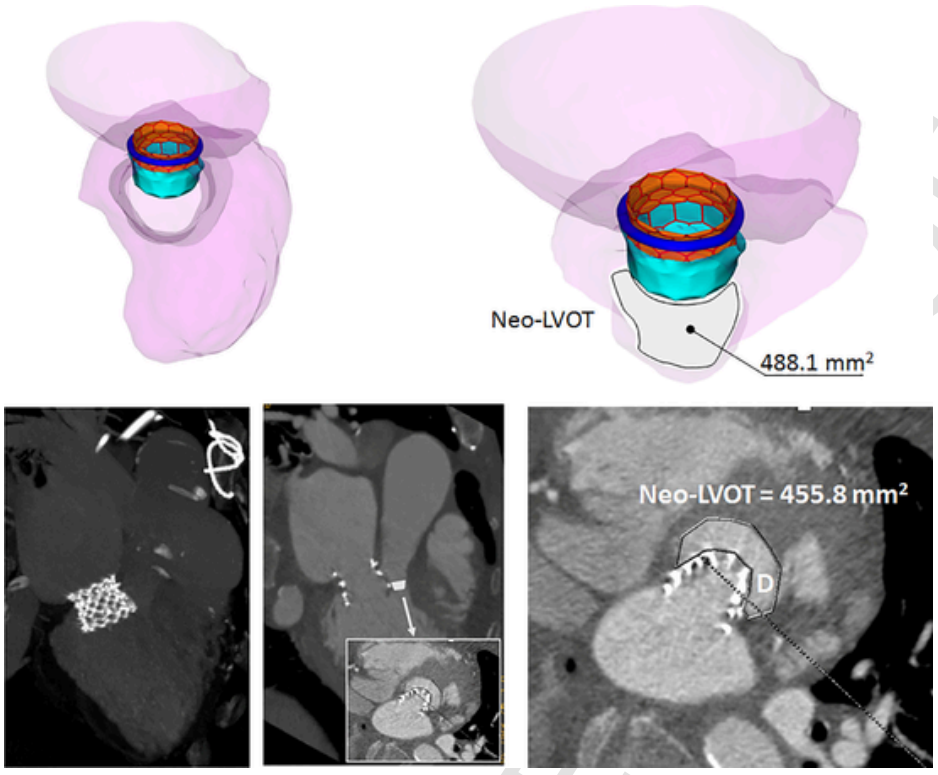

Fig. 6. 3D view of LVOT obstruction from the ascending aorta and corresponding neoLVOT area of Patient A (top) and post-TMVR CT measurements of neoLVOT area for Patient A.

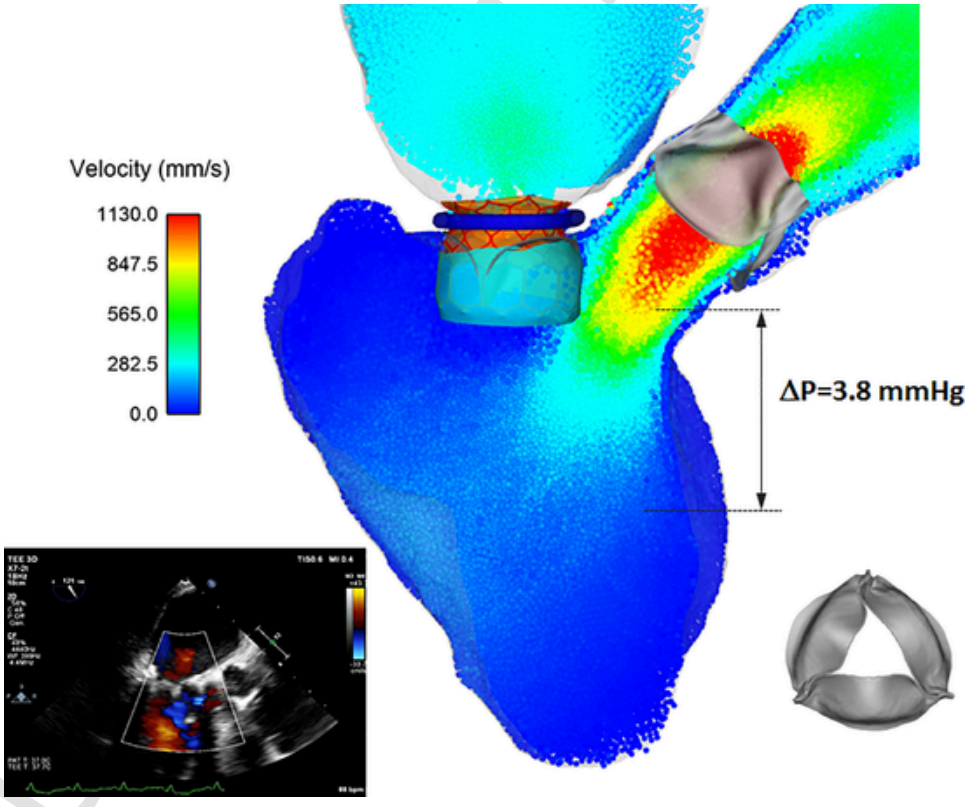

Fig. 7. Particle flow during systolic acceleration showing sub-aortic stenosis and pressure drop measurement for Patient B; the inset on the left shows TEE imaging.

these studies did not include the heart wall compliance or accounted for specific THV characteristics and deformed configurations. To our knowledge, this study is the first application of patient-specific modeling of TMVR to offer insights into the post-implantation hemodynamic and structural mechanics of left ventricle. The simulation of S3 Ultra deployment was based on finite-element analyses inspired by the mod-

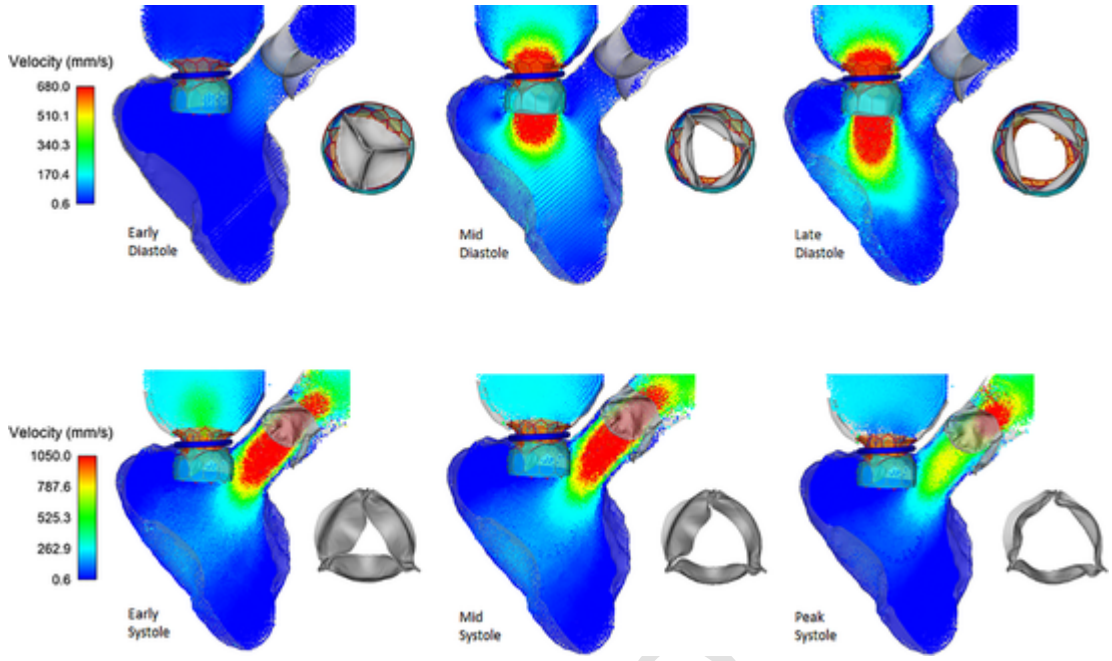

Fig. 8. Particle flow over the cardiac cycle for Patient A showing opening of both S3 Ultra and aortic valve.

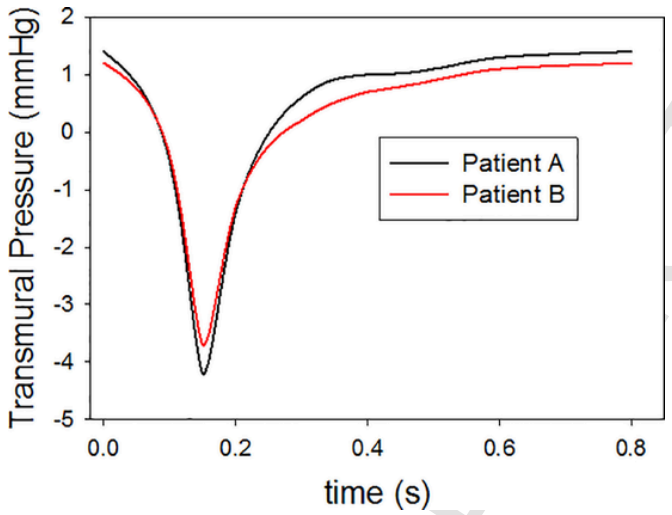

Fig. 9. Profile of transmural pressure exerted by the fluid on the anterior MV leaflet over the cardiac cycle; a negative transmural pressure pushes the anterior MV leaflet to the THV frame.

eling of transcatheter aortic valve implantation and includes the presence of the expandable balloon and the fluid-cavity approach for a faithfully replicate of the clinical procedure [25, 26]. The SPH method was successfully implemented to simulate the interaction between the blood flow and the S3 Ultra. The commercial code permitted a full integration of fluid particles with finite-element model components of THV deployment, with the interaction between the fluid and the solid handled by a general contact algorithm without additional effort to guarantee the kinematic of both the mitral and aortic valves. As a result, the simulation framework allowed us to show the final configuration of neoLVOT area and flow patterns in the left ventricle while the accuracy of simulation findings was evaluated by comparison with post-TMVR CT and TEE imaging.

There are areas for improvements in our modeling framework, and further validation of our results are also warrant to confirm the efficacy of TMVR in patients with less suitable left ventricular anatomy. The heart wall compliance was included in the SPH modeling by linear elastic material properties and thus not taking into consideration the true passive and active behavior of left ventricle. Caballero et al. [29] adopted cine-magnetic resonances (MR) images at different cardiac phases to prescribe the left ventricular motion in the SPH simulation. This approach is based on a template mesh for the computational domain of the left ventricle, which is inflated to match the endocardial surface seen at different cardiac phases from cine-MR imaging. Biffi et al. [30] developed a similar approach where a user-defined subroutine was implemented in ABAQUS to impose the MRI-derived nodal displacements of the left heart seen during the cardiac beating. Systolic flow here presented is likely underestimated because the myocardium was passively inflated by the atrial and aortic pressure loads. Indeed, the left ventricular volume between systole and diastole is limited due to the lack of active contraction. Both patients had left ventricular dysfunction (eg, end-diastolic volume of 208 ml and end-systolic volume of 175 ml for Patient B), suggesting limited myocardial contractility at systole. To improve convergence, FSI was not allowed for the annuloplasty band ring that likely undergoes substantial motion during cardiac beating. To improve convergence, FSI was not allowed for the annuloplasty band ring that likely undergoes substantial motion during cardiac beating. The lack of precise material properties information has induced us to consider the 3D Memo annuloplasty ring as a uniform and rigid hyperplastic material. However, the 3D Memo has a semi-rigid material behavior given by a non-planar shape with varying dimensions of Ni-Ti cell structure to obtain flexibility from the anterior to posterior portions of the ring. Simulation of a flexible ring design might shed light on a different adaptation of S3 Ultra to the failed annuloplasty ring. We do not foresee any issue in improving our model with ring data as soon as this information becomes available from a mechanical characterization of the 3D Memo ring. With regards to SPH modeling, the flow velocity could be affected by the pressure boundary conditions imposed by the rigid plates on the blood volume. To fully capture the dynamic response of LVOT obstruction, the modeling approach should be improved taking into account the presence of the chordae, pupillary muscles as well as the pressure loading from the right heart imparting motion of inter-ventricular septum. In future studies, these

aspects can be tackled by using a more complex and realistic model of the heart anatomy and improving the FSI approach here presented.

5. Conclusion

Using a patient-specific computational framework, we have elucidated the biomechanical implications of the neoLVOT as determined by a prolonged S3 Ultra to treat a failed annuloplasty ring. This is particularly relevant in TMVR, where LVOT obstruction is associated with a high rate of procedural adverse events. Quantitative hemodynamic and structural variables were derived from simulations and compared to those measured by both CT and TEE imaging to verify model fidelity. Predictions of neoLVOT area, alterations in the sub-aortic flow structure and pressure loads may help identify patients at high risk for LVOT obstruction, in whom pre-emptive clinical procedures like percutaneous laceration of anterior MV leaflet are recommended to decrease hemodynamic impairment due to a permanently-displaced MV after TMVR.

Uncited references

[31].

Declaration of Competing Interest

None

Funding

None

Ethical Approval

Not required

References

[1] S H Yoon, B K Whisenant, S Bleiziffer, V Delgado, N Schofer, L Eschenbach, et al. Transcatheter Mitral Valve Replacement for Degenerated Bioprosthetic Valves and Failed Annuloplasty Rings. J Am Coll Cardiol 2017;70:1121–1131.
[2] M Guerrero, D Dvir, D Himbert, M Urena, M Eleid, D D Wang, et al. Transcatheter Mitral Valve Replacement in Native Mitral Valve Disease With Severe Mitral Annular Calcification: results From the First Multicenter Global Registry. JACC Cardiovascular interventions 2016;9:1361–1371.
[3] D W M Muller, R S Farivar, P Jansz, R Bae, D Walters, A Clarke, et al. Transcatheter Mitral Valve Replacement for Patients With Symptomatic Mitral Regurgitation: a Global Feasibility Trial. J Am Coll Cardiol 2017;69:381–391.
[4] P Blanke, C Naoum, D Dvir, V Bapat, K Ong, D Muller, et al. Predicting LVOT Obstruction in Transcatheter Mitral Valve Implantation: concept of the Neo-LVOT. JACC Cardiovascular imaging 2017;10:482–485.
[5] S Alsidawi, M F Eleid, C S Rihal, V T Nkomo, S Pislaru Significant LVOT obstruction after mitral valve in ring procedure. Eur Heart J Cardiovasc Imaging 2015;16:1389.
[6] S H Yoon, S Bleiziffer, A Latib, L Eschenbach, M Ancona, F Vincent, et al. Predictors of Left Ventricular Outflow Tract Obstruction After Transcatheter Mitral Valve Replacement. JACC Cardiovascular interventions 2019;12:182–193.
[7] A Rinaudo, S Pasta Regional Variation of Wall Shear Stress in Ascending Thoracic Aortic Aneurysms. Proceedings of the Institution of Mechanical Engineers, Part H: Journal of Engineering in Medicine, 228; 2014. p. 627–638.
[8] S Pasta, J A Phillippi, A Tsamis, A D'Amore, G M Raffa, M Pilato, et al. Constitutive modeling of ascending thoracic aortic aneurysms using microstructural parameters. Med Eng Phys 2016;38:121–130.
[9] J J Lee, G D'Ancona, A Amaducci, F Follis, M Pilato, S Pasta Role of Computational Modeling in Thoracic Aortic Pathologies -A Review. J Card Surg 2014;29:653–662.
[10] G D'Ancona, A Amaducci, A Rinaudo, S Pasta, F Follis, M Pilato, et al. Haemodynamic predictors of a penetrating atherosclerotic ulcer rupture using fluid–structure interaction analysis. Interact Cardiovasc Thorac Surg 2013;17:576–578.
[11] S Pasta, G Gentile, G M Raffa, D Bellavia, G Chiarello, R Liotta, et al. In Silico Shear and Intramural Stresses are Linked to Aortic Valve Morphology in Dilated Ascending Aorta. European Journal of Vascular and Endovascular Surgery 2017;(17):30331–30333. S1078-5884.
[12] X Shen, T Wang, X Cao, L Cai The geometric model of the human mitral valve. PLoS ONE 2017;12:e0183362.
[13] S Pasta, G Gentile, G M Raffa, F Scardulla, D Bellavia, A Luca, et al. Three-dimensional parametric modeling of bicuspid aortopathy and comparison with computational flow predictions. Artif Organs 2017;41:E92–E102.
[14] Rinaudo A., D'Ancona G., Lee J.J., Pilato G., Amaducci A., Baglini R., et al. Predicting Outcome of Acute Aortic Dissection with Patent False Lumne by Computational Flow Analysis Cardiovascular Engineering and Technology. 2014;5:176–88.
[15] S Pasta, S Cannata, G Gentile, M Di Giuseppe, F Cosentino, F Pasta, et al. Simulation study of transcatheter heart valve implantation in patients with stenotic bicuspid aortic valve. Med Biol Eng Comput 2020.
[16] L Fratini, G Macaluso, S Pasta Residual stresses and FCP prediction in FSW through a continuous FE model. Journal of Materials Processing Technology 2009;209:5465–5474.
[17] J Bailey, N Curzen, N W Bressloff Assessing the impact of including leaflets in the simulation of TAVI deployment into a patient-specific aortic root. Comput Methods Biomech Biomed Engin 2016;19:733–744.
[18] S Morganti, N Brambilla, A S Petronio, A Reali, F Bedogni, F Auricchio Prediction of patient-specific post-operative outcomes of TAVI procedure: the impact of the positioning strategy on valve performance. J Biomech 2016;49:2513–2519.
[19] W Mao, A Caballero, R McKay, C Primiano, W Sun Fully-coupled fluid-structure interaction simulation of the aortic and mitral valves in a realistic 3D left ventricle model. PLoS ONE 2017;12:e0184729.
[20] S Morganti, M Conti, M Aiello, A Valentini, A Mazzola, A Reali, et al. Simulation of transcatheter aortic valve implantation through patient-specific finite element analysis: two clinical cases. J Biomech 2014;47:2547–2555.
[21] C Kleinstreuer, Z Li, C A Basciano, S Seelecke, M A Farber Computational mechanics of Nitinol stent grafts. J Biomech 2008;41:2370–2378.
[22] F Auricchio, M Conti, S Morganti, A Reali Simulation of transcatheter aortic valve implantation: a patient-specific finite element approach. Comput Methods Biomech Biomed Engin 2014;17:1347–1357.
[23] W Mao, K Li, W Sun Fluid-Structure Interaction Study of Transcatheter Aortic Valve Dynamics Using Smoothed Particle Hydrodynamics. Cardiovasc Eng Technol 2016;7:374–388.
[24] K Lavon, G Marom, M Bianchi, R Halevi, A Hamdan, A Morany, et al. Biomechanical modeling of transcatheter aortic valve replacement in a stenotic bicuspid aortic valve: deployments and paravalvular leakage. Med Biol Eng Comput 2019;57:2129–2143.
[25] A Finotello, S Morganti, F Auricchio Finite element analysis of TAVI: impact of native aortic root computational modeling strategies on simulation outcomes. Med Eng Phys 2017;47:2–12.
[26] G Luraghi, F Migliavacca, A Garcia-Gonzalez, C Chiastra, A Rossi, D Cao, et al. On the Modeling of Patient-Specific Transcatheter Aortic Valve Replacement: a Fluid-Structure Interaction Approach. Cardiovasc Eng Technol 2019;10:437–455.
[27] M Bianchi, G Marom, R P Ghosh, O M Rotman, P Parikh, L Gruberg, et al. Patient-specific simulation of transcatheter aortic valve replacement: impact of deployment options on paravalvular leakage. Biomech Model Mechanobiol 2019;18:435–451.
[28] K Kohli, Z A Wei, A P Yoganathan, J N Oshinski, J Leipsic, P Blanke Transcatheter Mitral Valve Planning and the Neo-LVOT: utilization of Virtual Simulation Models and 3D Printing. Curr Treat Options Cardiovasc Med 2018;20:99.
[29] A De Vecchi, D Marlevi, D A Nordsletten, I Ntalas, J Leipsic, V Bapat, et al. Left ventricular outflow obstruction predicts increase in systolic pressure gradients and blood residence time after transcatheter mitral valve replacement. Sci Rep 2018;8:15540.
[30] A Caballero, W Mao, L Liang, J Oshinski, C Primiano, R McKay, et al. Modeling Left Ventricular Blood Flow Using Smoothed Particle Hydrodynamics. Cardiovasc Eng Technol 2017;8:465–479.
[31] B Biffi, M Gritti, A Grasso, E G Milano, M Fontana, H Alkareef, et al. A workflow for patient-specific fluid-structure interaction analysis of the mitral valve: a proof of concept on a mitral regurgitation case. Med Eng Phys 2019;74:153–161.

UNCORRECTED PROOF